# Shear-induced self-diffusion in a wall-bounded dilute suspension

Evgeny S. Asmolov*
*Central Aero-Hydrodynamic Institute, Zhukovsky, Moscow Region, 140180, Russia*
(Received 9 March 2008; published 30 June 2008)

Random migrations of non-Brownian neutrally buoyant particles in the flow of a dilute suspension in a periodic Couette cell is simulated on the basis of a dipole model. A diffusivity is due to far-field collective hydrodynamic interactions. Large-scale fluctuations of particle concentration induce fluid velocity disturbances with a length scale comparable to the cell size. The calculated self-diffusivity coefficient is linear in particle volume content and agrees well with the experimental data.

DOI: 10.1103/PhysRevE.77.066312 PACS number(s): 47.55.P−, 82.70.Kj, 47.11.Kb

## I. INTRODUCTION

Non-Brownian neutrally buoyant particles migrate randomly across the streamlines of a carrier flow in sheared suspensions at small Reynolds numbers [1–3]. Migrations are due to the hydrodynamic interactions between the particles which cause velocities to fluctuate about the mean values. The phenomenon was explained by irreversibilities of particle interactions. The trajectories of two isolated interacting spheres undergoing a shear flow are symmetric and reversible in the Stokes regime. After the spheres have separated, they return to their original streamlines. Interactions of three or more particles [4] or interactions of two rough spheres [5] break the symmetry and lead to net transversal displacements. The three-particle mechanism [4] requires the diffusivity $D_s$ to be quadratic in the particle volume content $\phi$, since the probability for a tracer particle to interact with two other close particles scales as $\phi^2$. For this reason the mechanism is relevant for dense suspensions. In the experiments for dilute suspensions [6], $D_s$ was found to be linear in particle volume fraction $\phi$. The rough-sphere model [5] gives correct linear dependence in $\phi$. However, the experimental value of the diffusivity [6] is an order of magnitude greater than the theoretical predictions.

A new mechanism of the diffusivity in a dilute suspension has been proposed very recently [7] for a wall-bounded shear flow. When an initial separation in the normal direction is small, the normal component of relative particle velocity may change the sign due to far-field interactions with the walls. As a result the particles do not pass each other but exchange their positions in the gradient direction. Reversing trajectories result in a particle cross-stream migration. The calculated diffusivity agrees quantitatively with the experimental value. Reversing trajectories prevent near-contact particle encounters, and particle separations in the flow and vorticity directions remain large compared to the particle radius $a'$, of the order of $0.2H'$ for typical experimental values, $\phi=0.01$, $a'/H'=0.025$ [6], where $H'$ is the separation between the walls. Such pairs are not isolated but always have neighbors, as the separations are comparable with an interparticle distance.

The diffusivity is calculated using the simulations of particle motion in a wall-bounded cell. Different numerical approaches based on the detailed treatment of flow field around each dispersed particle, e.g., accelerated Stokesian dynamics (ASD) [8] and the two-dimensional (2D) lattice-Boltzmann model (LBM) [9], were applied to simulate dense sheared suspensions, $\phi=0.1-0.5$. The number of particles in a system is typically 1000. Sierou and Brady [8] showed the importance of high particle numbers and long simulation time to predict correctly the diffusion coefficient.

In the present work the mechanism of the diffusivity in a dilute suspension due to long-range collective interactions is studied. Large-scale fluctuations of particle concentration induce fluid velocity disturbances with the length scale of order of the separation between the walls. A large-scale flow is simulated using a simplified model of point particles. The approach was applied previously to calculate the fluctuations in dilute sedimenting suspensions [10–12] when the particle effect is approximated by point forces. In sheared suspensions the effect of a freely rotating neutrally buoyant particle is equivalent to symmetric force dipole at large distances [13]. The equations governing disturbance flow and particle motion in a rectangular periodic cell bounded by two parallel no-slip walls are derived in Sec. II. They are solved in terms of Fourier series. The numerical results are discussed in Sec. III. Finally, they are summarized in Sec. IV.

## II. GOVERNING EQUATIONS

The motion of $N$ identical point particles in a rectangular cell is simulated. The $x$, $y$, and $z$ axes are directed along the undisturbed Couette flow, the velocity gradient and the vorticity, respectively, $\mathbf{e}_x$, $\mathbf{e}_y$, and $\mathbf{e}_z$ are the unit vectors. The cell is bounded by two rigid walls in the $y$ direction and periodic in two other directions. Non-Brownian particles are distributed randomly over the cell at $t=0$.

The governing equations are nondimensionalized using the distance between the walls $H'$ and the shear rate $\dot{\gamma}$. Particle velocity in a dilute suspension is assumed to be the sum of the velocity of the undisturbed Couette flow and large-scale disturbances due to particle effect. Then the equation of motion of $l$th particle is written as

*Also at Institute of Mechanics, Lomonosov Moscow State University, Moscow, Russia; aes@an.aerocentr.msk.su

 

$$\frac{d\mathbf{x}_l}{dt} = y_l \mathbf{e}_x + \mathbf{u}(t,\mathbf{x}_l), \quad l = 1, \ldots, N, \tag{1}$$

$$\mathbf{x}_l = (x_l, y_l, z_l), \quad \mathbf{x}_l(0) = \mathbf{x}_{l0},$$

$$\mathbf{u} = \sum_{j \neq l}^{N} \mathbf{u}_j(\mathbf{x}_j, \mathbf{x}_l). \tag{2}$$

Here $\mathbf{u}$ is a fluid velocity disturbance at the particle position $\mathbf{x}_l$ due to interactions with other particles. The effect of a particle freely rotating in a shear flow can be approximated at distances large compared to $a'$ by symmetric force dipole [13]. The local shear-rate induced by other particles in a dilute suspension is assumed to be small compared to the undisturbed value, so the dipole strength is constant for all particles. When the Reynolds number based on the cell size is small, the large-scale flow induced by $j$th particle is governed by the dimensionless Stokes equations

$$\nabla \cdot \mathbf{u}_j = 0,$$

$$\nabla p_j - \Delta \mathbf{u}_j = -S\left[\frac{\partial \delta(\mathbf{x}-\mathbf{x}_j)}{\partial y}\mathbf{e}_x + \frac{\partial \delta(\mathbf{x}-\mathbf{x}_j)}{\partial x}\mathbf{e}_y\right], \tag{3}$$

$$\mathbf{u}_j = 0 \quad \text{on } y = 0;1,$$

where $S = \frac{10}{3}\pi a^3$. The dimensionless particle radius $a$ is related with other groups by $a = (3\phi L_x L_z / 4\pi N)^{1/3}$, where $L_x$ and $L_z$ are the dimensionless sizes of the cell in the $x$ and $z$ directions, respectively.

The solution of linear equations (3) is constructed in terms of the 2D Fourier series. The similar approach has been applied for point particle forces sedimenting in a quiescent fluid [12]. The fluid flow is periodic in the $x$ and $z$ directions, so it can be sought for an arbitrary particle position in terms of Fourier series in the plane parallel to the walls, with the wave vectors commensurate with the cell sizes,

$$\mathbf{q}_j = \sum_{k_x,k_z} \mathbf{q}_j^* \exp[i(k_x x + k_z z)], \quad \mathbf{q}_j = (\mathbf{u}_j, p_j), \tag{4}$$

$$\mathbf{u}(t,\mathbf{x}_l) = \sum_{k_x,k_z} \left\{ \exp[i(k_x x_l + k_z z_l)] \sum_{j \neq l}^{N} \mathbf{u}_j^* \right\}, \tag{5}$$

$$k_{x,z} = m_{x,z} 2\pi / L_{x,z}, \quad m_i = 0, \pm 1, \pm 2, \cdots .$$

Substituting expansions (4) into Eq. (3) one obtains a system of ordinary differential equations (ODE) for $\mathbf{q}_j^*$:

$$\nabla^* \cdot \mathbf{u}_j^* = 0, \tag{6}$$

$$\nabla^* p_j^* - \Delta^* \mathbf{u}_j^* = -Sn_j^* \begin{pmatrix} d\delta(y-y_j)/dy \\ ik_x \delta(y-y_j) \\ 0 \end{pmatrix}, \tag{7}$$

$$\mathbf{u}_j^* = 0 \quad \text{on } y = 0;1, \tag{8}$$

$$\nabla^* = \left(ik_x, \frac{d}{dy}, ik_z\right), \quad \Delta^* = \frac{d^2}{dy^2} - k_\perp^2, \quad k_\perp^2 = k_x^2 + k_z^2,$$

$$n_j^* = \frac{\exp[-i(k_x x_j + k_z z_j)]}{L_x L_z}.$$

When $k_\perp = 0$ the solution of Eqs. (6)–(8) is simple,

$$u_{xj}^* = \begin{cases} -Sn_j^* y & \text{as } y \leqslant y_j, \\ -Sn_j^*(y-1) & \text{as } y > y_j, \end{cases}$$

$$u_{yj}^* = u_{zj}^* = 0 \quad \text{as } k_\perp = 0.$$

When $k_\perp \neq 0$ the system (6)–(8) can be reduced to a single ODE for the Fourier transform of the normal velocity,

$$\Delta^{*2} u_{yj}^* = -ik_x Sn_j^* \left[\frac{d^2\delta(y-y_j)}{dy^2} + k_\perp^2 \delta(y-y_j)\right], \tag{9}$$

$$u_{yj}^* = \frac{du_{yj}^*}{dy} = 0 \quad \text{on } y = 0;1. \tag{10}$$

The dipole approximation fails to describe the hydrodynamic interactions of close particles. However, we assume that large-scale disturbances with the length scale comparable to the cell size play a key role in a fluctuation evolution while interactions at distances of the order of particle size are of less importance. For this reason there is no need to resolve small scales for which the dipole model gives only crude representation.

A numerical treatment of the problem requires a truncation of the Fourier series (4) with a number of harmonics great enough to resolve properly the evolution of large-scale fluctuations. Truncated series result in a smoothing of the concentration and velocity fields in the $x$ and $z$ directions. To smooth the particle effect on large-scale flow in the normal direction one can present the singularity on the right-hand side of Eq. (9) in terms of truncated Fourier series in $y$,

$$-ik_x Sn_j^* \left[\frac{d^2\delta(y-y_j)}{dy^2} + k_\perp^2 \delta(y-y_j)\right] = -ik_x S \sum_{k_y} (k_\perp^2 - k_y^2)\tilde{n}_j \exp(ik_y y),$$

$$\tilde{n}_j(t,\mathbf{k}) = \frac{\exp(-i\mathbf{k}\cdot\mathbf{x}_j)}{L_x L_z}, \quad \mathbf{k} = (k_x, k_y, k_z), \quad k_y = 2\pi m_y.$$

Then the solution of the fourth-order ODE (9) is

$$u_{yj}^* = -ik_x S \sum_{k_y} \frac{(k_\perp^2 - k_y^2)\tilde{n}_j}{k^4} \exp(ik_y y) + \sum_{n=1}^{4} a_n^y \varphi_n, \tag{11}$$

$$k^2 = k_x^2 + k_y^2 + k_z^2, \quad \varphi_{1,2} = \exp(\pm k_\perp y), \quad \varphi_{3,4} = y \exp(\pm k_\perp y).$$

Here $\varphi_j$ are the solutions of the homogeneous equation (9). The four unknown constants $a_n^y$ are found uniquely in order

to satisfy four boundary conditions (10). The equations governing the Fourier coefficients of other velocity components can be also derived from Eqs. (6) and (7),

$$\Delta^* u_{xj}^* = -iSk_z \sum_{k_y} \frac{[k_y^2 k^2 + k_x^2(k_\perp^2 - k_y^2)]\tilde{n}_j \exp(ik_y y)}{k^2 k_\perp^2} - 2ik_x \sum_{n=1}^{2} a_{n+2}^y \varphi_n, \quad (12)$$

$$\Delta^* u_{zj}^* = 2iSk_x k_z \sum_{k_y} \frac{k_y \tilde{n}_j \exp(ik_y y)}{k^2} - 2ik_z \sum_{n=1}^{2} a_{n+2}^y \varphi_n. \quad (13)$$

Their solutions are sought similar to Eq. (11) with the four unknown constants $a_{1,2}^{x,z}$ to be found from the no-slip conditions on the walls.

The velocity disturbance induced by a single particle in a cell is zero with a high degree of accuracy at the particle position $\mathbf{x}=\mathbf{x}_j$. This means that the possible particle self-effect is negligible, and one may calculate a single sum $\Sigma_j^N \mathbf{u}_j^*$ over all particles in Eq. (5), rather than the sum $\Sigma_{j\neq l}^N \mathbf{u}_j^*$ for each particle $l$.

## III. NUMERICAL RESULTS

An initial particle distribution over the cell may be either homogeneous or inhomogeneous. To form a homogeneous distribution we seed randomly nonoverlapping spheres over the whole volume. An inhomogeneous distribution can be assigned by seeding of some particle portion into a smaller volume. The equations of particle motion (1) are integrated using the fourth-order Runge-Kutta routine with the time step $\Delta t=0.01$. The dimensionless particle radius is $a=2.5\times10^{-2}$, which is the same as the experimental value [6]. Most results are obtained for the cell sizes $L_x=L_z=2$ and the average particle content $\phi=10^{-2}$. The corresponding particle number in the cell, $N=3\phi L_x L_z/4\pi a^3=611$, is comparable with the particle number in the ASD [8] and LBM [9] calculations. The disturbance velocity is evaluated using Eqs. (4) and (11) with the sums truncated at some cutoff number $m_{\max}$, so that all modes with $|m_y|\leqslant m_{\max}$ and $|m_i|\leqslant m_{\max}L_i, i=x,z$, are taken into account. Large $m_{\max}$ makes the evaluation of the truncated sums in Eqs. (4) and (11)–(13) computationally expensive. The total number of the modes is $N_m=(2m_{\max}+1)(2m_{\max}L_x+1)(2m_{\max}L_z+1)\propto m_{\max}^3$, and the number of operations grows like $NN_m\propto Nm_{\max}^3$. Different $m_{\max}=2-6$ are tried in the calculations of the diffusivity. The usual cutoff number is $m_{\max}=4$ and $N_m=2601$.

### A. Particle trajectories

The disturbance velocity given by the dipole approximation differs from the exact solution in the Stokes regime [14] at small distances. As a result trajectories of two isolated, interacting spheres also differ from the exact ones when an initial cross-stream separation is small. However, the dipole representation of the Stokes flow retains the reversibility property, which is important when calculating migration across streamlines. Figure 1 shows typical trajectories of one particle relative to the pair midpoint $\mathbf{x}_0-y_0t\mathbf{e}_x$ in the $(x,y)$ plane. The cell sizes are $L_x=L_z=2$, $m_{\max}=6$, initial particle positions are $\mathbf{x}_{10}=(\mathbf{x}_0-\delta\mathbf{x}_0/2)$, $\mathbf{x}_{20}=(\mathbf{x}_0+\delta\mathbf{x}_0/2)$, with $\delta x_0=1$ and different $y_0$, $\delta y_0$, $\delta z_0$. The trajectories are passing and symmetric when the initial separations in the gradient direction $\delta y_0$ are greater than a critical value. They are reversible, and such interactions do not contribute to the diffusivity. Small oscillations are due to the periodic particles and series truncation.

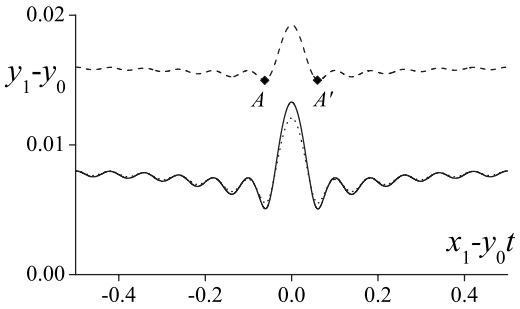


FIG. 1. Passing trajectories of isolated particle pairs. Trajectories start at $y_0=0.6$, $\delta x_0=1$, $\delta y_0=0.016$, $\delta z_0=0$ (solid line), $\delta y_0=0.032$, $\delta z_0=0$ (dashed line), $\delta y_0=0.016$, $\delta z_0=0.032$ (dotted line). Time required to pass a distance from point $A$ to $A'$ is 6.5.

Another class of reversing or swapping trajectories has been found recently for linear shear flow between walls either in the Stokes [7] or in the finite-inertia [15,16] regimes. The normal component of the relative particle velocity changes the sign at small $\delta y_0$. As a result the particles initially approach each other, then move across the streamlines, reverse their directions, and separate without passing each other. The swapping trajectories result in net particle cross-stream displacements. This migration mechanism has been proposed [7] as an explanation of the enhanced hydrodynamic self-diffusivity in dilute suspensions.

Particle separations on the reversing trajectories remain always large compared to the particle radius. The swapping effect is due to long-range pair and wall-particle interactions and can be described using the dipole model. Figure 2 shows the trajectories calculated for the same normal separation and different transverse separations. The reversing trajectories in

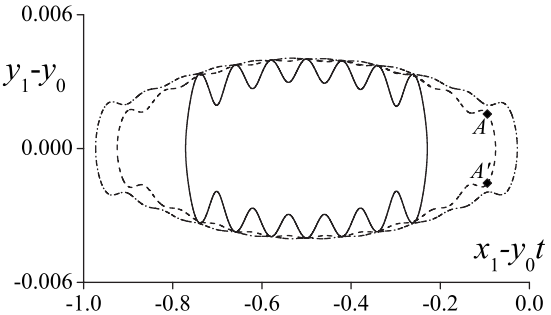


FIG. 2. Reversing trajectories of isolated particle pairs are closed in the periodic system. Trajectories start at $y_0=0.6$, $\delta x_0=1$, $\delta y_0=0.008$, $\delta z_0=0, 0.2, 0.3$ (solid, dashed, and dashed-dotted lines, respectively). Time required to pass a small distance from point $A$ to $A'$ is long, $t_{rev}=45$.

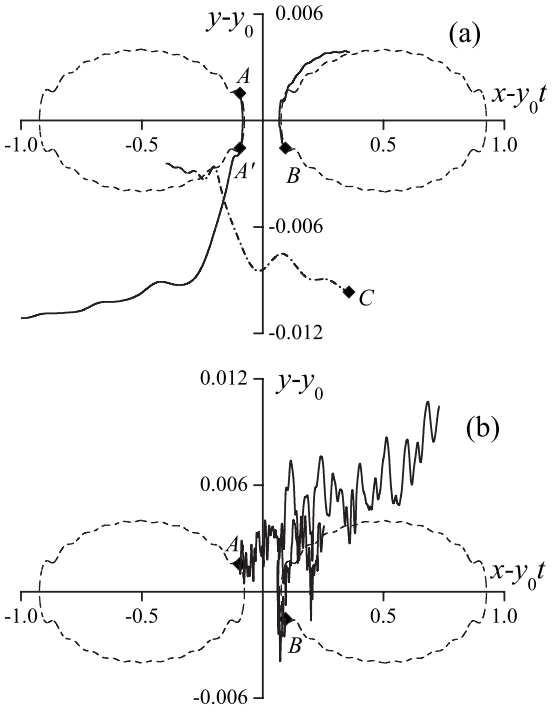


FIG. 3. Effect of other particles on reversing pair trajectories. Dashed lines are the trajectories of the isolated pair placed initially at $A$ and $B(\delta z_0^{AB}=0.2)$. Other particles are seeded randomly over the cell. (a) Pair trajectories (solid lines) due to the interactions with closest neighbor (particle $C$, $\delta z_0^{AC}=0.104$). Dashed-dotted line is the trajectory of particle $C$. (b) Pair trajectories due to the interactions with all particles in the cell.

the periodic system, unlike the system infinite in the $x$ direction, are closed and remain reversible. The period is large, $T_{st}=384$, for $\delta y_0=0.008$, $\delta z_0=0$ (solid line in Fig. 2). The first particle approaches the second one, then moves in the opposite direction and interacts with periodically replicated opposite particle. It returns to the original streamline because of the antisymmetric interaction.

Typical particle separations in either the flow or the vorticity directions, $\delta x \sim \delta z \sim 0.2$, are comparable with the interparticle distance $(L_x L_z/N)^{1/3}$. Besides, an interaction time for reversing trajectories $t_{rev}=O(100)$ is much longer than that for passing trajectories. The dimensionless time required to pass a small distance from point $A$ to $A'$ on the reversing trajectory shown in Fig. 2 (dashed line) is 45, while that for the passing trajectory in Fig. 1 is 6.5. As a result the pair cannot be treated as an isolated even in the dilute suspension with $\phi=0.01$ and $a=0.025$. It has neighbors at comparable distances during the interaction. The effect of other particles on the pair is illustrated in Fig. 3. Two particles are placed initially at the points $A$ and $B(\delta z_0=0.2)$. The other 609 particles are seeded randomly over the cell. Dashed lines are the trajectories of the isolated pair when the effect of other particles is neglected (the same as the dashed trajectory in Fig. 1). Figure 3(a) shows the trajectories when the effect of only one closest neighbor (particle $C$) is taken into account. The simulation time is $t_{run}=300$. As the initial separation is small the pair trajectories in the three-particle system are close to the reversing trajectories until the first particle reaches the point $A'$. Then the first trajectory deviates significantly from the reversing trajectory due to the interaction with the particle $C$. Figure 3(b) presents the pair trajectories during $0 \leqslant t \leqslant 150$ when the interactions between all particles in the cell are taken into account. The pair normal velocities and positions vary fast and randomly due to long-range collective particle interactions. Large-scale concentration and velocity fluctuations correlate during a time $t_{cor}=O(1)$, required for particles separated by a distance of order $H'$ in the normal direction to translate a comparable distance relative to each other in the streamwise direction. $t_{cor}$ is much shorter than the time of reversing trajectories $t_{rev}=O(100)$. The interactions of particles $A$ and $B$ contribute to their displacements. However, multiple long-range interactions lead to a loss in memory of a relative pair position during $t_{cor}$. Thus the cross-stream migrations are due mainly to large-scale fluctuations. The same conclusion follows from the calculations of the mean-square displacements.

### B. Self-diffusivity

The self-diffusivity is evaluated as the time rate of change of half the mean-square displacements,

$$D_s = \frac{1}{2}\frac{d}{dt}\langle \Delta y \Delta y \rangle. \tag{14}$$

The displacements should be followed for very long times [8]. The simulation time is usually $t_{run}=400$. Even greater run time, $t_{run}=1200$, is chosen for the systems with less $N$ or $m_{\max}$. The self-diffusivity is evaluated from Eq. (14) using the linear best fits of the displacement curves. The mean-square displacements are calculated as functions of initial particle positions $y_{l0}$. The data are averaged over particles in slices $y_0-h_y<y_{l0}<y_0+h_y$, $h_y=0.05$ and over 30 runs. Figure 4 shows the displacements for a homogeneous initial particle distribution calculated for different $y_0$ as functions of time. It should be reminded that $\langle \Delta y \Delta y \rangle$ and $D_s$ are scaled using the separation between the walls rather than the particle radius. The curves are similar qualitatively to those obtained by ASD [8] and LBM [9] for dense suspensions. The dependences are quadratic in time initially. Such a behavior corresponds to the regime when particle positions are still strongly correlated. After a time $t=O(1)$ the curves show the linear behavior corresponding to the diffusive regime. The slopes are close for particles starting in the middle part of the cell. The diffusivity is less for particles close to the walls as the velocity disturbances are zero on the walls. The time necessary for the diffusive regime to be reached is independent of $\phi$ [see Fig. 4(b)]. ASD simulations [8] reported approximately the same value of the transient time for dense suspensions. It was assumed that the transient time should be large in very dilute suspensions as the interactions of close particles are seldom. However, within the present mechanism of the diffusivity, the correlations in the positions of distant particles are important. As a result a loss in memory occurs during the correlation time $t_{cor}=O(1)$ regardless of the particle concentration.

Figure 5 presents the diffusivity in the median slice of the cell, $0.4 \leqslant y_{l0} \leqslant 0.6$, as functions of the cell sizes, or the pe-

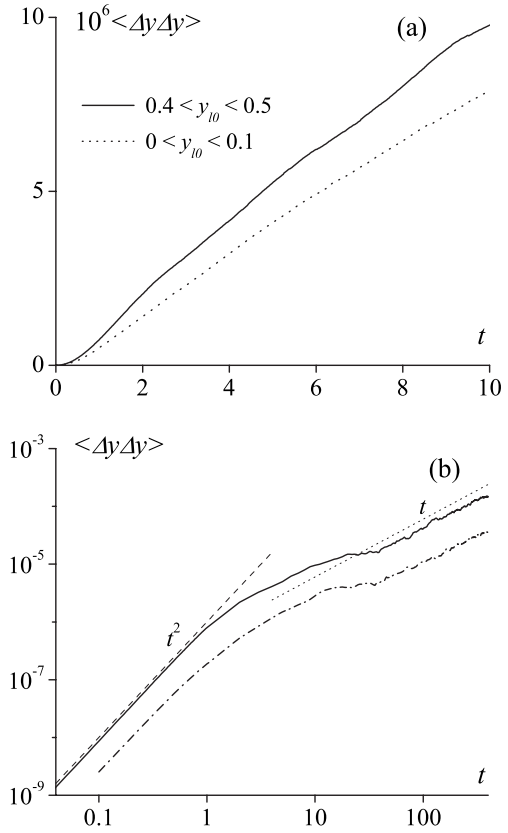


FIG. 4. (a) The mean-square displacements as a function of time for different initial particle positions $y_{l0}$ and $\phi=10^{-2}$. (b) Log-log plots for particles in the median slice, $0.4<y_{l0}<0.5$, $\phi=10^{-2}$ (solid line), and $\phi=3\times10^{-3}$ (dashed-dotted line). The times necessary for the diffusive regimes (linear dependences) to be reached are comparable for different $\phi$.

riods in the two directions. Periodic images influence significantly on the particle migrations when they are located at distances comparable to the separation between the walls. A sharp increase can be seen for small sizes in the flow direction (Fig. 5). The dependence on the size in the vorticity direction exhibits an opposite trend. The diffusivity is approximately constant for the cell sizes in both directions greater than 2. The reason is that the normal velocity disturbance between no-slip walls decays exponentially at

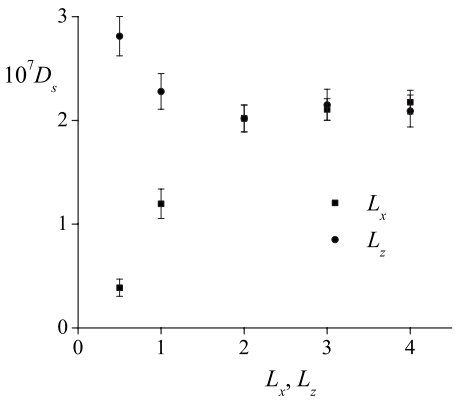


FIG. 5. Effect of the cell sizes on the diffusivity.

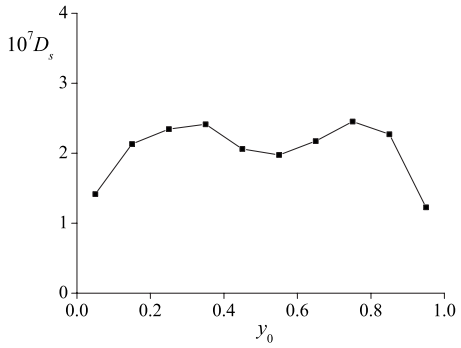


FIG. 6. Self-diffusivity in a homogeneous suspension at $\phi=10^{-2}$ as a function of initial particle position $y_{l0}$.

large distances [17] when $L>1$. The simulations with small periods $L_x\leqslant1$ exclude the long-wave harmonics $\mathbf{k}=\pi(1,m_y,m_z/L_z)$. The figure thus supports the assumption that large scales are most important for the diffusivity in a dilute suspension. Different truncations of Fourier series lead to the same conclusion since $D_s$ enhances only slightly when $m_{\max}>4$.

The diffusivity in dense suspensions is attributed to short-range interactions of close particles. However, a strong dependence on the system size similar to the dependence on $L_x$ in Fig. 5 was also observed for dense 3D ($\phi=0.35$) [8] and 2D ($\phi=0.25$) [9] systems. The diffusivity grows with the particle number when $N<200$. It was concluded [9] that the effect is due to particle interactions with their periodic images. The distance between the periodic particles was large, $L_x\simeq35.4a\simeq0.5$ at $\phi=0.25$, $N=200$ (the distance between the walls was kept constant at $71a$). Hence long-range interactions may be important in evaluating the diffusivity even for dense suspensions.

Figure 6 shows the self-diffusivity in a homogeneous suspension at $\phi=10^{-2}$, $L_x=L_z=2$ as a function of initial particle position. A local minimum is obtained at the center of the cell where the diffusivity is usually measured in the experiments. The average value for particles in the median slice, $0.4\leqslant y_{l0}\leqslant0.6$, is $D_s=2.02\times10^{-7}\pm1.3\times10^{-8}$. The diffusivity is also less for particles close to the walls because of the no-slip conditions for fluid velocity disturbances. Even though the diffusivity varies across the cell width, the average concentration remains uniform since the particle migrations during the simulation time $t_{run}$ are small, $\Delta y\sim\sqrt{D_s t_{run}}<0.01$ [see also Fig. 4(b)].

A nonuniform concentration may be assigned artificially. To form inhomogeneous initial distribution we seed randomly 5% of the total particle number into the middle section of the cell, $1/3<y_{l0}<2/3$, and the remaining particles uniformly over the whole cell. Even small concentration inhomogeneity (solid line in Fig. 7) produces significant change in the diffusivity (cf. Figs. 6 and 7). One would expect that the diffusivity is proportional to the local concentration, if migrations are caused by a local mechanism such as pair interactions on reversing trajectories. However, the diffusivity increases far from the region of enhanced concentration, at the distances 0.1–0.2 from the walls. This requires the diffusivity in dilute suspensions to be due to a global mechanism such as large-scale fluctuations.

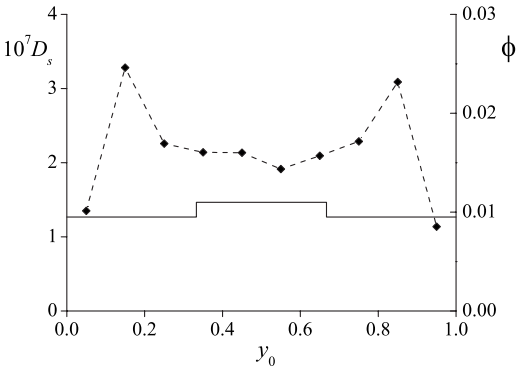


FIG. 7. Self-diffusivity vs particle position $y_{l0}$ (dashed line) for nonuniform concentration (solid line). $D_s$ increases significantly far from the region of enhanced concentration, for particles near the walls, $0.1<y_{l0}<0.2$, $0.8<y_{l0}<0.9$.

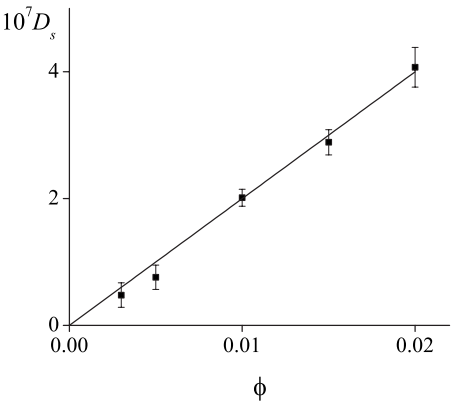


FIG. 8. Self-diffusivity in the median slice, $0.4<y_{l0}<0.6$, of a homogeneous suspension as a function of particle volume fraction (symbols). The line is a linear best fit.

The self-diffusivity is evaluated for different particle volume fraction. The dependence $D_s(\phi)$ for particles in the median slice is shown in Fig. 8. In the experiments [6], $D_s$ was found to be linear in $\phi$, and $D_s/\phi=2.25\times10^{-5}$. Theoretical dependence is also linear. The best fit gives $D_s/\phi\approx2\times10^{-5}$ which is close to the experimental value. The linear dependence can be readily explained within the fluctuation mechanism of the diffusivity following to the speculations by Caflisch and Luke for a sedimenting suspension [18]. The number fluctuations $\Delta n$ for particles distributed randomly are $O(N^{1/2})$. As a result one has $D_s\propto\langle u^2\rangle\propto\langle\Delta n^2\rangle\propto N\propto\phi$.

## IV. CONCLUSIONS

The shear-induced diffusion in a dilute suspension of non-Brownian neutrally buoyant particles has been considered. The suspension flow in a periodic Couette cell has been simulated based on the dipole approximation. Both reversible passing and reversing trajectories of an isolated pair are obtained within the model. Collective long-range interactions lead to a loss in memory of a relative pair position during a time $O(1)$.

The diffusivity is due to the large-scale fluctuations in particle concentration and fluid velocity rather than long-term pair interactions on reversing trajectories. The diffusivity in a homogeneous suspension is linear in the particle volume content. The model compares well with the experimental data [6]. The self-diffusivity varies across the cell width. The maxima are at the distances $0.3H'-0.4H'$ from the walls. Even small concentration inhomogeneity results in a significant diffusivity growth near the walls.

## ACKNOWLEDGMENT

This work was supported by Russian Foundation for Basic Research (Grant No. 05-01-00847).

[1] E. C. Eckstein, D. G. Bailey, and A. H. Shapiro, J. Fluid Mech. **79**, 191 (1977).
[2] D. Leighton and A. Acrivos, J. Fluid Mech. **177**, 109 (1987).
[3] G. Bossis and J. F. Brady, J. Chem. Phys. **87**, 5437 (1987).
[4] Y. Wang, R. Mauri, and A. Acrivos, J. Fluid Mech. **327**, 255 (1996).
[5] F. R. Da Cunha and E. J. Hinch, J. Fluid Mech. **309**, 211 (1996).
[6] I. E. Zarraga and D. T. Leighton, Phys. Fluids **14**, 2194 (2002).
[7] M. Zurita-Gotor, J. Blawzdziewicz, and E. Wajnryb, J. Fluid Mech. **592**, 447 (2007).
[8] A. Sierou and J. F. Brady, J. Fluid Mech. **506**, 285 (2004).
[9] J. Kromkamp, D. V. D. Ende, D. Kandhai, R. V. D. Sman, and R. M. Boom, J. Fluid Mech. **529**, 253 (2005).
[10] L. Bergougnoux, S. Ghicini, E. Guazzelli, and E. J. Hinch, Phys. Fluids **15**, 1875 (2003).
[11] P. J. Mucha, S.-Y. Tee, D. A. Weitz, B. I. Shraiman, and M. P. Brenner, J. Fluid Mech. **501**, 71 (2004).
[12] E. Asmolov, Fluid Dyn. **42**, 410 (2007).
[13] P. G. Saffman, J. Fluid Mech. **22**, 385 (1965).
[14] G. K. Batchelor and J. T. Green, J. Fluid Mech. **56**, 375 (1972).
[15] Y. Yan, J. Morris, and J. Koplik, Phys. Fluids **19**, 113305 (2007).
[16] P. M. Kulkarni and J. F. Morris, J. Fluid Mech. **596**, 413 (2008).
[17] N. Liron and S. Mochon, J. Eng. Math. **10**, 287 (1976).
[18] R. E. Caflisch and J. H. C. Luke, Phys. Fluids **28**, 759 (1985).